PNAS RESEARCH ARTICLE | ANTHROPOLOGY ENGINEERING

Advanced materials engineering in historical gypsum plaster formulations

Moslem Mishmastnehi[a,1], Alexander E. S. Van Driessche[b,c], Glen J. Smales[d], Alicia Moya[b], and Tomasz M. Stawski[d,1]

Edited by Elisabetta Boaretto, Weizmann Institute of Science, Rehovot, Israel; received May 23, 2022; accepted December 25, 2022 by Editorial Board Member Lia Addadi

We show how historical gypsum plaster preparation methods affect the microstructure and the wettability properties of the final stucco materials. We reproduced a traditional Persian recipe (*Gach-e Koshteh,* ~14th century AD), which involves a continuous mechanical treatment during plaster hydration. These samples were compared with a laboratory-replicated historical recipe from Renaissance Italy (*Gesso Sottile,* ~15th century AD) and contemporary low-strength plaster. The *Koshteh* recipe induces the formation of gypsum platelets, which exhibit preferential orientation in the plaster bulk. In contrast, the Italian and low-strength plasters comprise a typical needle-like morphology of gypsum crystals. The platelets in *Koshteh* expose the more hydrophilic {010} face of gypsum in a much more pronounced manner than needles. Consequently, the Iranian plaster displays enhanced wettability, enabling its direct use for water-based decoration purposes, or as a fine finishing thin layer, without the need of mixing it with a binder material. Contrary, in *Sottile,* gypsum crystals are left to equilibrate in large excess of water, which promotes the growth of long needles at the expense of smaller crystals. Typically, such needles are several times longer than those found in a control regular plaster. For this crystal habit, the total surface of hydrophilic faces is minimized. Consequently, such plaster layers tend to repel water, which can then be used, e.g., as a substrate for oil-based panel paintings. These findings highlight the development of advanced functional materials, by tuning their microtexture, already during the premodern era.

gypsum | plaster | *Sottile* | Persian | *Koshteh*

Significance

Based on oral interviews with artists, and preserved written sources, we replicated gypsum paste formulations used in historical artworks: *Gach-e Koshteh* from ~14th century AD in Iran and *Gesso Sottile* from ~15th century in Italy. We show that the obtained additive-free gypsum plasters display a more hydrophilic character if we follow the *Koshteh* method and a more hydrophobic character if the *Sottile* approach is used. These differences are caused by the changes in the crystallographic texture of the material and reveal an astonishing technical achievement in a historical context. The findings reported here confirm that there is an unknown body of technical data that can contribute to the development of improved sustainable preservation and restoration methods for the gypsum-containing cultural objects.

Gypsum ($CaSO_4{\cdot}2H_2O$) is an abundant and easily accessible mineral on the Earth's surface (1) and is extensively used as a source for building materials. The production procedure has, fundamentally, not changed since prehistoric times and involves the heat treatment of gypsum rock at ~200 °C, inducing dehydration and recrystallization to hemihydrate ($CaSO_4{\cdot}0.5H_2O$, bassanite or "plaster of Paris"). The hemihydrate yields a workable paste when mixed with water and solidifies within a few minutes (2). The hardening process relies on bassanite gradually rehydrating and recrystallizing back to gypsum (3, 4). The final hardened plaster is typically composed of interlocking micrometer-sized gypsum needles (5, 6).

The archeological record points to applications of gypsum as mortar and plaster dating back to the Neolithic period in the geographical regions of what are now Iran, Cyprus, and Egypt (7–10). Other use cases of calcium sulfate involve the application of a thin layer of gypsum on the exterior surface of ceramic pots from the fourth to third millennium BC in Harappa (Punjab, Pakistan) (11) or its usage for different purposes such as a repair material for ceramics, rock relief and statues, and pigment or molding material from ancient Egypt before the Greco-Roman period (years 332 BC to 395 AD) (8–10). Later on, in medieval and Renaissance Italy, the use of gypsum as a molding material was widespread. Numerous devotional polychrome reliefs are known to be made in the workshops of masters, such as Donatello and Ghiberti. Such reliefs were likely copied by molding a gypsum-based material from an original model made of bronze or marble (12). Italy is also known for advanced processing routines of gypsum, where craftspeople applied gypsum as a specific substrate for paintings. For example, in the 15th to 16th centuries AD, the so-called *Gesso Sottile* was used to prepare an impregnation underlayer for panel paintings or gilding (13, 14). This well-documented technique is also known as *Gesso Mate* or *Gesso Fino* in the Iberian peninsula and has been also practiced in this region for a long time (15, 16). *Gesso Sottile* was generally prepared by slowly suspending plaster of Paris in an excess volume of water (the order of 5 g bassanite in 1,000 g water). This mixture was frequently stirred for an extended period of time (hours, days, or even months), with the water usually refreshed several times, until a very fine suspension was obtained. In the next steps, this suspension was decanted, deposited, and dried. In addition, the as-prepared fine gypsum powder (*Sottile*) was mixed with animal glue, as a binder

Author contributions: M.M. and T.M.S. designed research; M.M., A.E.S.V.D., and T.M.S. performed research; M.M., A.E.S.V.D., G.J.S., A.M., and T.M.S. contributed new reagents/analytic tools; M.M., A.E.S.V.D., G.J.S., A.M., and T.M.S. analyzed data; and M.M., A.E.S.V.D., and T.M.S. wrote the paper.

The authors declare no competing interest.

This article is a PNAS Direct Submission. E.B. is a guest editor invited by the Editorial Board.

[1]To whom correspondence may be addressed. Email: mmishmast@gmail.com or tomasz.stawski@bam.de.

This article contains supporting information online at https://www.pnas.org/lookup/suppl/doi:10.1073/pnas.2208836120/-/DCSupplemental.

Published February 10, 2023.

phase, to achieve a white, ivory-like surface for painting or a smooth substrate for gilding (13, 17). Considering the relatively elaborate preparation route for *Gesso Sottile* and its use as the final underlayer before the painting layer, the Renaissance painters most likely employed this specific treatment of gypsum because it was advantageous, e.g., for better adhesion of their paintings and gilding layers.

Most noticeably, in the historic region of Persia, the application of gypsum plaster for decoration reached a very high level of skill, and the preserved artifacts point to approximately two millennia of continuous usage (18–20). Although the implementation of gypsum-based stucco revetments on buildings had already began during the Sasanian era (years 224 to 651 AD) (18), it was not until the early Islamic period (since the 9th century AD) that gypsum utilization reached an advanced level of design and execution (20). The recipe for *Gach-e Koshteh*, literally "killed gypsum" in Persian, has survived through oral tradition among stucco masters until present-day Iran (21, 22) (*SI Appendix*, Text 1). This formulation relies on intentional processing, involving kneading and pressing (for details, see *Materials and Methods* and Movie S1), and in contrast to the European counterpart, the concept behind *Gach-e Koshteh* was to prepare underlayers for pigmentation and painting on the wall without any additional glue.

In contrast to other anthropogenic materials, such as metal, glass, or ceramic, extracting information from gypsum to reconstruct past human activities is very limited. For the production of historical materials, we can typically identify and/or hypothesize the existence of distinct steps or traceable changes between raw materials and the final products (23–25). However, in the case of gypsum, the raw material and the final product, e.g., plaster, are very alike, making it very challenging to pinpoint the specific treatment methods and to correlate it with the materials' properties. Currently, it is well understood that bassanite converts to gypsum through a dissolution–reprecipitation mechanism (2, 3), i.e., the hemihydrate phase dissolves, and the dihydrate phase nucleates and grows as a new crystalline phase. This de novo crystallization implies that 1) a new microstructure of the gypsum-based material is obtained, and 2) the microstructure could be engineered via the physicochemical conditions of the processes, e.g., water content and temperature. In turn, the resulting microstructures could influence the surface properties of the plaster material, such as its interactions with water. So far, no studies have established (21) a link between the microstructural properties of the used gypsum paste and a particular treatment for a specific form of decoration. Thus, in this work, our aim is to reveal how specific historical recipes for gypsum paste preparation, from Iran and Europe, potentially affect the microstructure of the final plasters and their surface wetting properties when replicated in the laboratory. We used a combination of advanced bulk and surface-sensitive techniques to characterize in detail the microstructural features of different laboratory-prepared samples and compared those results with historical samples of *Gach-e Koshteh*.

Materials and Methods

Laboratory-Prepared Samples. The starting materials for all the laboratory-prepared samples were high-purity bassanite ($CaSO_4 \cdot 0.5H_2O$, Sigma Aldrich, >99.99%) and deionized water (Milli-Q, >18 MΩ). The gypsum pastes were prepared following the *Gesso Sottile, Gach-e Koshteh*, and a common method for low-strength plaster, as is detailed below. For the preparation of the *Gesso Sottile* material, we replicated the processes as historically described (13, 14, 16), making necessary adjustments and interpretations of a 500-y-old recipe. In *Gesso Sottile,* an excess of water is the key: 5 g bassanite was dispersed in 1,000 g water, which corresponded to a stoichiometric bassanite-to-water ratio of ~1:1,600. This dispersion was stirred using a glass spatula for 60 s and left to sediment over ~16 h. In the next step, most of the supernatant was removed by decantation, so that ~50 mL of a slurry was left. The slurry was poured into petri dishes (10 cm in diameter) and left to dry at 30 °C in air for 24 h. Consequently, a very soft yet continuous thin plaster layer was obtained.

The recipe of *Gach-e Koshteh* plaster was based on oral interviews with stucco masters in Iran (*SI Appendix*, Text 1). It requires approximately a bassanite-to-water ratio of 1:1 by mass, which translates to a stoichiometric ratio of ~1:8 and implies ~5.3-fold excess in the amount of water necessary to convert bassanite to gypsum ($CaSO_4 \cdot 2H_2O$). Overall, plaster prepared from such a composition would be of low strength (in terms of Young's modulus and maximal bending) and of high porosity in comparison with low–water content counterparts, where the highest mechanical strength is achieved for a bassanite-to-water ratio of typically ~2:1 (6, 26). On the other hand, the used water content provides increased fluidity and workability of the paste and as such is traditionally used to make Koshteh. We typically mixed 50 g bassanite with 50 g water to obtain 100 g of a paste. The preparation method described below is also documented in a video (Movie S1). This video also contains footage from a thermal camera (Optris PIX 400 camera, OPT PIX Connect ver. 3.16 software), which was used to identify crucial stages of the process related to temperature changes in the gypsum paste. The temperature displayed on screen corresponded to the maximum values measured in Area 1 at a given moment of time, while the color scale was kept constant for a predefined range of 18 to 40 °C. Traditionally, the changes in temperature were sensed manually by a stucco master preparing the paste (21). We conducted the first mechanical treatment of the paste, i.e., stirring for ~8 min followed by pressing and squeezing the paste to prevent it from the final setting for 8 to 10 min (Movie S1). During the initial ~8 min, the calcium sulfate–water mixture gradually increased in viscosity without any noticeable temperature increase (T = ~20 °C). After this period of time, the paste reached soft solid consistency which made it suitable for further processing by hand (*SI Appendix*, Text 1). During the subsequent mechanical treatment (after the initial 8 min), the temperature of the paste gradually increased up to T = ~39 °C after ~11 min. The mechanical treatment needed to be continued beyond this point after which the paste gradually cooled. At this stage, a small amount of water (~2 mL in our case) was added to adjust the workability of the paste (Movie S1, 10 min 47 s). Finally, the material was deposited onto a surface and left to harden and dry. As a part of the final step, the processed paste was divided into 10 batches that were put onto glass petri dishes and left to dry at 30 °C in air for 24 h.

In a third set of experiments, by following the procedure above, we prepared a series of 4 time-resolved samples. These samples were collected at 0-, 2-, 4-, and 8-min intervals of mechanical processing and left to set at 30 °C in air for 24 h. The samples were obtained in chunks of ~10 g in weight each. In this regard, the first sample was taken just after stirring (of ~8 min), before any further mechanical treatment, while the last sample corresponded to a final *Gach-e Koshteh*. Therefore, the first untreated sample (at 0 min) serves as our unprocessed low-strength plaster control used as a starting point for a *Koshteh* recipe. In this regard, as mentioned, our plaster control is of lower strength than a typical plaster which would be made using a higher bassanite-to-water ratio and would not be stirred or agitated during the initial setting processes.

Historical Samples. We compare the microstructural features observed in our laboratory-replicated samples with selected (and available) historical materials. Two gypsum-based samples were collected from historical architectural decorations in Iran belonging to the 13th to 15th centuries AD. The first sample (labeled StB-102) was collected from the substrate of the mural painting in the dome chamber of the *Sheikh Ahmad-e Jami* mausoleum complex in Torbat-e jam (35.247122°N, 60.628986°E). It was previously presumed that this substrate was made by the application of the *Koshteh* recipe (21, 27), and therefore, it is one of the main historical samples in our study. The second sample (labeled StB-27) is from an innovative type of stucco decoration, the so-called *Appliqué* plaster (*Fetilehey* or *Pish-Sakhteh*), which was collected from *Sayyid Rukn al-Din* mausoleum in Yazd (31.901040°N, 54.369762°E). This is a unique technique of stucco decoration that appears in central Iran no earlier than the 14th and 15th centuries AD. The procedure in which the gypsum paste is prepared for this technique is referred to as "half-way" *Koshteh* and includes long-term stirring of a water–plaster mixture and involves an addition of polysaccharides and clay into the mix, followed by limited mechanical treatments before its implementation on

the wall (28). This partial application of the *Koshteh* recipe, according to previous research and the interviewed local stucco masters (*SI Appendix*, Text 1 and ref. 28), makes this sample a relevant addition to be considered within this study.

Diffraction/Scattering Methods. The phase and crystallographic texture of the samples were characterized using transmission X-ray diffraction. Wide-angle X-ray scattering measurements were performed using the MOUSE instrument (29) equipped with a microfocus X-ray Mo tube (Kα, λ = 0.71073 Å) and multilayer optics (spot size of 643 μm (fwhm)). Scattered radiation was detected on an in-vacuum Eiger 1 M detector (Dectris, Switzerland), which was placed at ca. 52 mm from the sample. The use of a two-dimensional (2D) detector allowed for straightforward observation of anisotropic diffraction patterns associated with crystallographic textures in the samples. The resulting data were processed using DAWN (30, 31) software package (v. 2.20). We converted the 2D patterns to polar coordinates ("cake" plots) to compare the intensities in different directions by integrating the direction-dependent diffracted intensities to 1D curves as is described elsewhere (32).

Complementary texture analysis of the laboratory-made *Koshteh* and *Sottile* plaster samples was performed by measuring a series of 2D X-ray diffraction patterns (33) using a BRUKER SMART APEX diffractometer equipped with an APEX CCD area detector. The pole figures of the 020 reflection were generated for each sample from 72, 2D patterns collected every 5° by rotating the sample around the ϕ axis (in plane) and by processing the diffractograms in XRD2DScan software (34).

Atomic Force Microscopy and Spectroscopy (AFM/AFS). AFM/AFS measurements were conducted with a MFP-3D microscope from Asylum Research. The maximum range of the piezo scanner was 120 μm in the planar direction (*x,y*) and 15 μm in the vertical direction (*z*). The microscope was isolated inside a chamber and was mounted on top of a vibration isolation control unit from Herzan. Topography images were acquired in contact mode with triangular silicon nitride (PNP-TR from NanoWorld) cantilevers with a nominal length of 100 μm, width of 13.5 μm, and thickness of 500 nm. AFM probes had a nominal spring constant of 0.35 N/m and were calibrated before each AFM measurement using the thermal method (35). The tip deflection sensitivity was determined by fitting the linear region of the force–distance curves obtained in a glass slide and resulting in 90 to 110 nm/V.

For AFS measurements, triangular silicon nitride (Au-PNP-TR from NanoWorld) cantilevers were used, identical to those used for AFM imaging (i.e., same cantilever dimensions and spring constants), but with a coating of Cr (5 nm, inner layer) and of Au (30 nm, outer layer). The gold on the tip surface enabled for their further functionalization with thiol molecules by formation of self-assembling monolayers (36). In particular, the functionalization protocols involved cleaning of the gold-coated AFM tips with UV/O_3 for 20 min, and immediately after, the tips were immersed for 24 h into 5 mM $HS(CH_2)_{10}CH_3$ and $HS(CH_2)_{10}COOH$ dissolved in pure ethanol (all chemicals provided by Merck). Thus, we obtained CH_3- and COOH-terminated tips that were used to measure their interaction force (adhesion) with the mineral surface.

Using the functionalized tips, hydrophobic and hydrophilic interaction forces with the mineral surface were explored in the three gypsum-based plasters by using CH_3- and COOH-tips, respectively. We measured 5 to 10 areas of 5 × 5 μm^2 by acquiring for each map 32 × 32 force–distance curves with the two different functionalized AFM tips while scanning the sample surface for 12 min. We measured all the force–distance curves from 1-μm distance from the surface, with a maximum normal load of 5 nN, 0.1 s of dwell time on the surface, and a tip velocity of 4 μm/s for the tip approaching and retracting. As a result, we simultaneously obtained topographical and adhesion force maps with a resolution of 150 nm/pixel. All measurements were carried out at room temperature. The obtained data were processed using AR and WSxM software (37). The comparison of the samples was performed following the statistical methods described in the *SI Appendix*: Supplementary Note 2. The individual adhesion force values are collected in Dataset S2.

Scanning Electron Microscopy (SEM). SEM imaging was performed with several instruments: Carl Zeiss SMT Ultra 55 Plus and Supra 40 field emission scanning electron microscopes, as well as Carl Zeiss LEO 1450 equipped with a tungsten filament source. Samples were typically coated with carbon before imaging. Images were further processed in ImageJ2 (38). A false-color map was applied to all images.

Gas Adsorption and Porosimetry. The specific surface area of the selected samples was derived from the gas adsorption measurements. The calculations were done on the adsorption branch of the isotherm using the method of Brunauer, Emmett, and Teller (39). For the experiments, Micromeritics ASAP 2010 was used, and the adsorption isotherms were measured with nitrogen at 77 K until the relative pressure range $p/p_0 = 0.5$. The porosity of the plaster samples was determined by means of the mercury intrusion porosimetry performed with a Micromeritics AutoPore V instrument. The measurements in the low pressure range were conducted from 0.0036 to 0.3 MPa and in the high pressure up to 400 MPa, where the pore diameter is inversely proportional to the applied pressure following the Washburn equation (40). The used pressure ranges allowed for a predicted pore size distribution from ~3.6 nm to 400 μm.

Gas adsorption and porosity measurements were performed on the samples from the third set of experiments (see Laboratory-Prepared Samples), namely, 4 time-resolved *Koshteh* samples collected at 0-, 2-, 4-, and 8-min intervals. The raw data from gas adsorption and porosimetry in the form of machine-generated reports are included as a Dataset S1 (file: Supporting_Dataset 1_MIP_and_BET_data.pdf). These reports also contain specific measurement conditions used for each sample.

Results

The different laboratory-prepared plaster samples were characterized by SEM to determine the morphology of the gypsum crystals. Representative electron micrographs from the three main types of gypsum plaster are shown in Fig. 1. Low-strength plaster is predominantly composed of needle-shaped crystals with an aspect ratio of ~10:1 (up to ~10 μm long and ~1 μm thick; Fig. 1*A*). The crystals appear to exhibit a relatively broad size distribution, and a large number (>50%) of smaller needle crystals are also visible (<1 μm in length). The *Gesso Sottile* sample (Fig. 1*B*) has a microstructure quite similar to that of low-strength plaster, but the needles appear to be more idiomorphic and larger. Prismatic crystals are clearly visible (~10 to 30 μm long and ~1 μm thick), with the presence of smaller crystals (<1 μm in length) greatly reduced. The growth of such large needles has led to a less dense distribution than observed in regular plaster (Fig. 1*A*). *Gach-e Koshteh* exhibits a significantly different morphology compared with both low-strength plaster and *Gesso Sottile* samples (Fig. 1*C*). Crystals have platelet shape (typically up to ~6 μm long and ~3 μm wide), whose aspect ratios (~2:1 to 5:1) are significantly lower than those observed with the needles. The platelets are more densely packed (in comparison with Fig. 1 *A* and *B*), conferring the appearance of a compacted structure.

In Fig. 2, the crystallographic properties of low-strength plaster, *Gesso Sottile,* and *Gach-e Koshteh* are compared. The presented diffraction patterns confirm that the investigated plasters are made of gypsum ($CaSO_4{\cdot}2H_2O$; *SI Appendix*, Fig. S1), and no significant amount of any other calcium sulfate phase is present. Diffraction patterns from low-strength plaster (Fig. 2*A*) and *Gesso Sottile* (Fig. 2*B*) are very similar to each other. In both cases, intensities along the azimuthal directions are relatively constant (rows I and II). Indeed, the 1D diffraction patterns integrated for several possible centroids and averaged over entire diffraction patterns (see labels in Fig. 2 *A* and *B*, rows III and IV) show that regardless of the azimuthal angle the diffraction patterns are essentially isotropic. In both cases, the highest intensities are observed at q of 1.47 $Å^{-1}$ which corresponds with index (12-1). The *Koshteh* sample (Fig. 1*C*), on the other hand, appears significantly different from the other two recipes, where the diffraction pattern is highly anisotropic (rows I and II). Integration of the 2D patterns around the high-intensity centroids in the azimuthal angle and their 90° low-intensity counterparts (rows III and IV) shows that the high-intensity direction is dominated by the 0.83 $Å^{-1}$ peak (row III), while for low-intensity azimuthal angles, the 1.47 $Å^{-1}$ peak

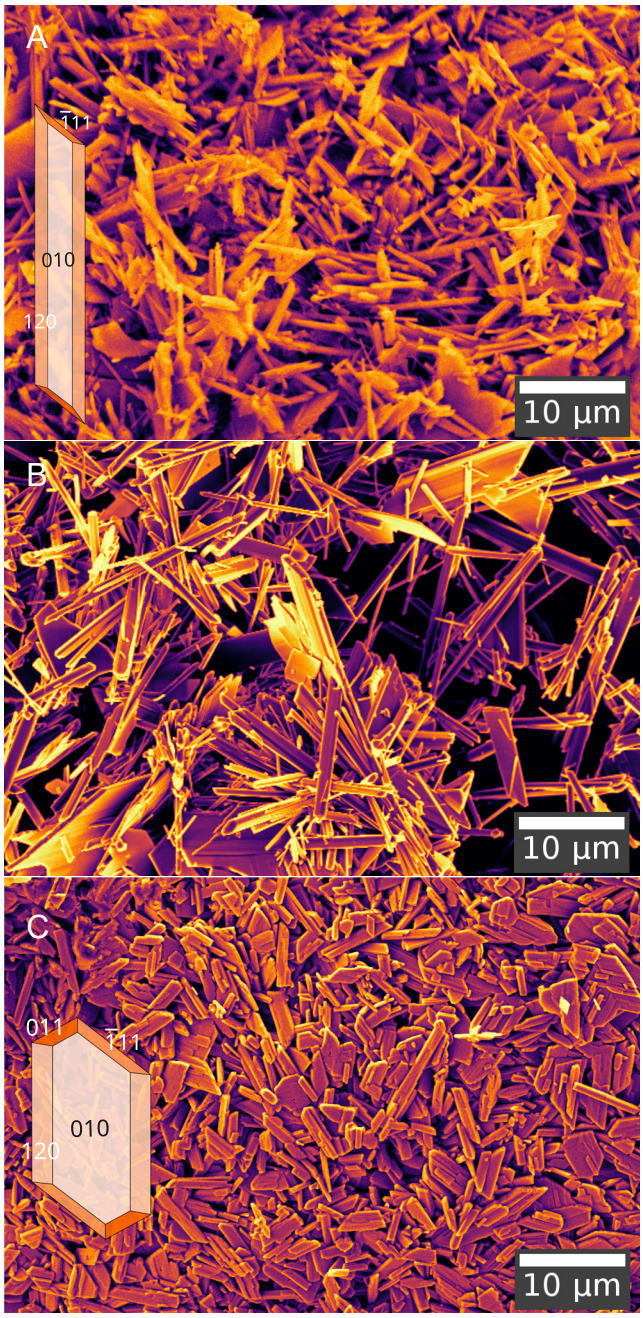

Fig. 1. Scanning electron micrographs measured with an in-lens detector from (*A*) low-strength regular plaster; 10 keV; (*B*) *Gesso Sottile*; 5 keV; and (*C*) *Gach-e Koshteh*; 5 keV. In *A* and *C*, representations of typical needle and platelet gypsum morphologies are shown indicating the main crystallographic faces.

has the highest intensity (row IV). The peak at q of 0.83 Å^{-1} has index (020). The changes in relative peak intensities between *Koshteh* and regular/*Sottile* samples suggest that the average crystal morphology is different for these samples (38), which is in line with the SEM observations (Fig. 1). Moreover, the highly anisotropic diffraction pattern of *Koshteh* seems to indicate a preferential orientation and texture of the {010} facets (41–43), which is confirmed through complementary 2D X-ray diffraction data collected from the surface of *Koshteh* and *Sottile* samples (*SI Appendix*, Fig. S2). Pole figures along the (020) reflection (*SI Appendix*, Fig. S2*A*) reveal a preferential orientation and texture of the {010} faces approximately parallel to the external plaster surface for *Koshteh*, while no specific surface texture was observed in the (020) pole figure of the *Sottile* samples. 1D diffraction patterns (*SI Appendix*, Fig. S2*B*), obtained through radial integration of the 2D data, display a similar change in relative peak intensity of the (020) and (12-1) reflections as those shown in Fig. 2.

Overall, the SEM and diffraction data demonstrate that low-strength plaster and *Gesso Sottile* samples are mainly composed of needle-shaped crystals which do not exhibit any specific texture (i.e., random crystal orientation), while *Gach-e Koshteh* is composed of platelet-shaped crystals displaying a texture dominated by the alignment of {010} facets which are compacted parallel to the external plaster surface.

To provide further details on the texture generation of *Koshteh* plaster, 2D diffraction patterns were collected at different time points (0, 2, 4, and 8 min) during the mechanical processing of a *Koshteh* sample (Fig. 3 *A*–*D* and Movie S1). Hence, Fig. 3*A* corresponds to the pattern of low-strength plaster, as found in Fig. 2*A*, whereas Fig. 3*D* represents the final *Koshteh* after 8 min of mechanical processing. In the case of low-strength plaster (Fig. 2*A*), the intensity along the azimuthal direction is relatively constant, and the peak at 1.47 Å^{-1} is the most intense one (the pink profile in row II). As the material is manually processed, the texture effects become visible at 2 min (Fig. 3*B*), which is evidenced by the ever-increasing amplitude in the diffraction profiles along the azimuthal direction (compare 0.83 Å^{-1} peak, the black profile in row II of Fig. 3 *A* and *B*). Further processing of 4 and 8 min makes this anisotropic effect even more pronounced. In addition, the mechanical treatment introduces strong anisotropy, which causes the peak at 0.83 Å^{-1} to reach the maximum intensity at two equivalent azimuthal positions (centroids at ~−135° and ~+45° in Fig. 3*C*; ~0° and ~±180° in Fig. 3*D*) and two decrease in intensity with minimas at positions 90° away. For the maximum intensity positions, the 0.83 Å^{-1} peak is ~3 times more intense than the 1.47 Å^{-1} peak. The changes depicted in Fig. 3 point to two simultaneous effects caused by the mechanical treatment. First, the crystals get oriented in a specific direction, which is likely correlated with the shearing movement during the mechanical treatment and resulting in texture (Movie S1): when gypsum is pressed and sheared between the palms in a repetitive manner. Second, the fact that the 0.83 Å^{-1} peak becomes dominant over the one at 1.47 Å^{-1} for certain directions implies that the crystals change their shape in agreement with Fig. 1: from needles to platelets. Importantly, the changes displayed in Fig. 3 *A*–*D* are also accompanied by a gradual decrease in the materials' surface area (from 2.2 m^2/g at 0 min to 1.7 m^2/g after 8 min; *SI Appendix*, Fig. S3) and the reduction in porosity (from ~71 to 49%; see *SI Appendix*, Fig. S3). Considering the simultaneous reduction in porosity and surface area, we can conclude that mechanical processing and the associated change in crystal morphologies lead to a denser and better-packed plaster microstructure.

AFM/AFS of Different Plaster Samples. The topography of low-strength plaster, *Gesso Sottile,* and *Gach-e Koshteh* samples (analogous to Figs. 1–3) was characterized using atomic force microscopy (AFM) in contact mode. Representative height and deflection images shown in Fig. 4 *A*–*F* reveal a transition from a surface morphology dominated by needle-shaped crystals in regular plaster and *Sottile* samples to a surface morphology dominated by platelet-shaped crystals in the *Koshteh* sample. The nanoscale wettability properties of the plaster surface were also explored by directly measuring the interaction (adhesion) force between functionalized AFM tips and the individual crystal surfaces. In particular, we obtained measurements of the hydrophobic and hydrophilic interactions with the plaster surface using CH_3- and COOH-tips, respectively. Each force map contains 30 × 30 force–distance curves and covers a spatial area of 5 × 5 µm^2, measuring thus the surface heterogeneity of the plaster formed by many gypsum crystals. Since the stacking

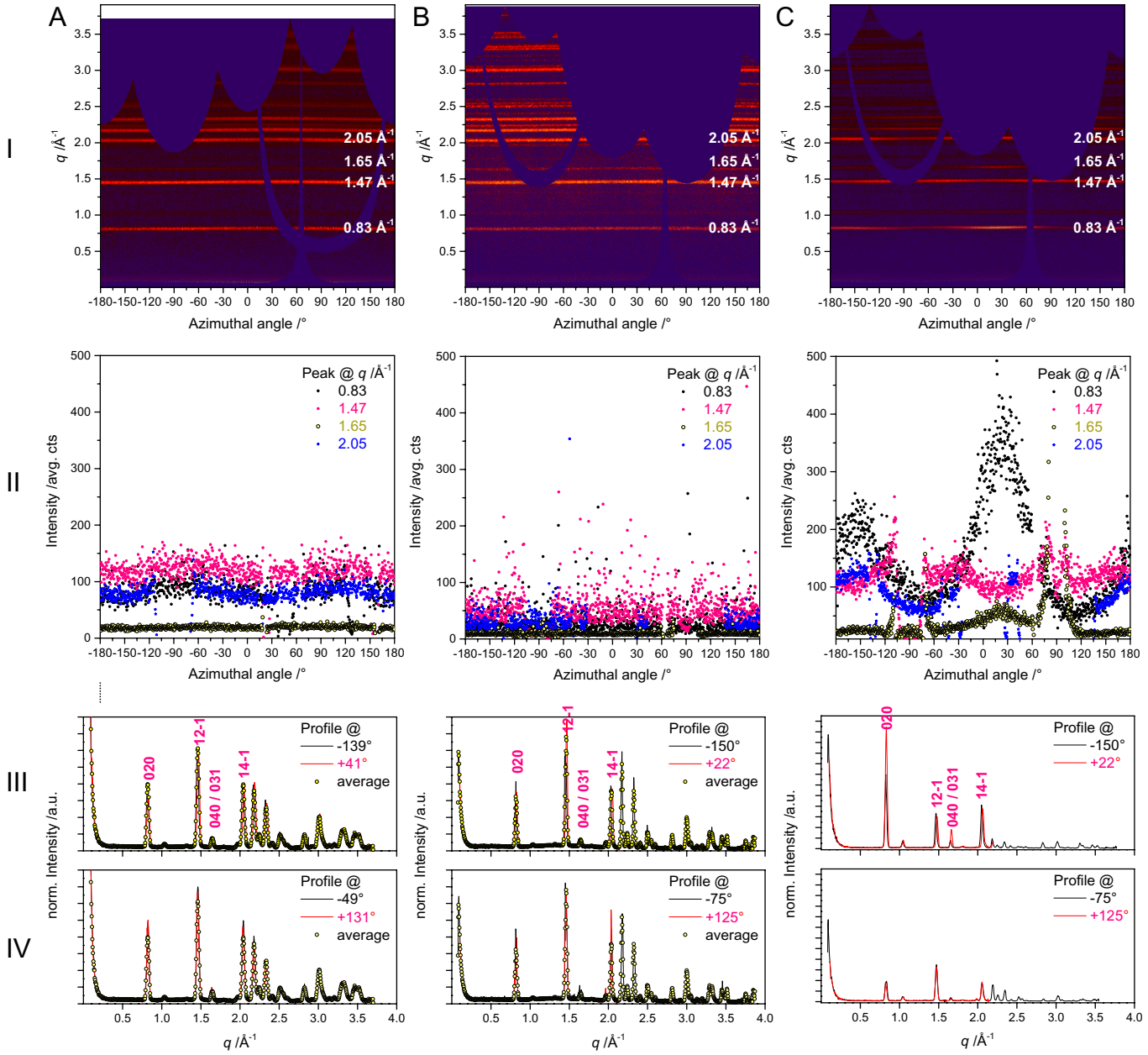

Fig. 2. Diffraction patterns measured for (*A*) low-strength typical plaster, (*B*) *Gesso Sottile*, and (*C*) *Gach-e Koshteh*. Row I: diffraction patterns are given in polar coordinates ("cake plots"), and the *q* positions of characteristic peaks are labeled. Row II: integrated profiles for each of the characteristic peaks. Rows III and IV: profiles integrated from I for selected azimuthal angles/directions as labeled. Please note that the azimuthal angle values in rows III and IV for *A* and *B*, for which the profiles were calculated, were purely arbitrary and irrelevant because the diffraction patterns were isotropic.

of the gypsum crystals leads to comparable surface roughness in all samples, we avoided very different contact areas between the AFM tip and the sample surface which is a crucial point for a correct comparison of the obtained values (44). Importantly, when comparing the topographical and force spectroscopy results (*SI Appendix*, Fig. S4), a correlation between the wettability (adhesion) properties and the different crystal morphologies becomes apparent. The platelet morphology characteristic for *Koshteh* corresponds to a more hydrophilic character of this sample (higher adhesion force with the COOH-tip), while the needle morphology characteristic of *Sottile* and low-strength plaster corresponds to a less hydrophilic behavior.

For each sample and each functionalized tip, 20 force maps were measured to establish a coherent view of the surface wettability. Fig. 4*G* presents the statistical results in a form of adhesion force histograms, which reveal a high surface heterogeneity as a consequence of the different exposed crystal facets. Yet, the results show that the predominance of platelet morphology in *Koshteh* sample improves the wettability of the plaster (higher hydrophilicity and higher adhesion forces with the COOH-tip) in comparison with the facets of the needle morphology characteristic of low-strength plaster and *Sottile*. In order to quantify the difference in wettability properties among the plaster samples, we performed a detailed statistical analysis (see *SI Appendix*: Supplementary Note 2). First, we applied a normality test and a homoscedasticity test, which showed *P*-values close to 0 for *Koshteh*, regular, and Sottile in both tests. Consequently, our data did not follow a normal distribution, which is very common in single-molecule techniques (45–47). To appropriately evaluate if there were significant differences in the wetting behavior of the plaster samples, we relied on

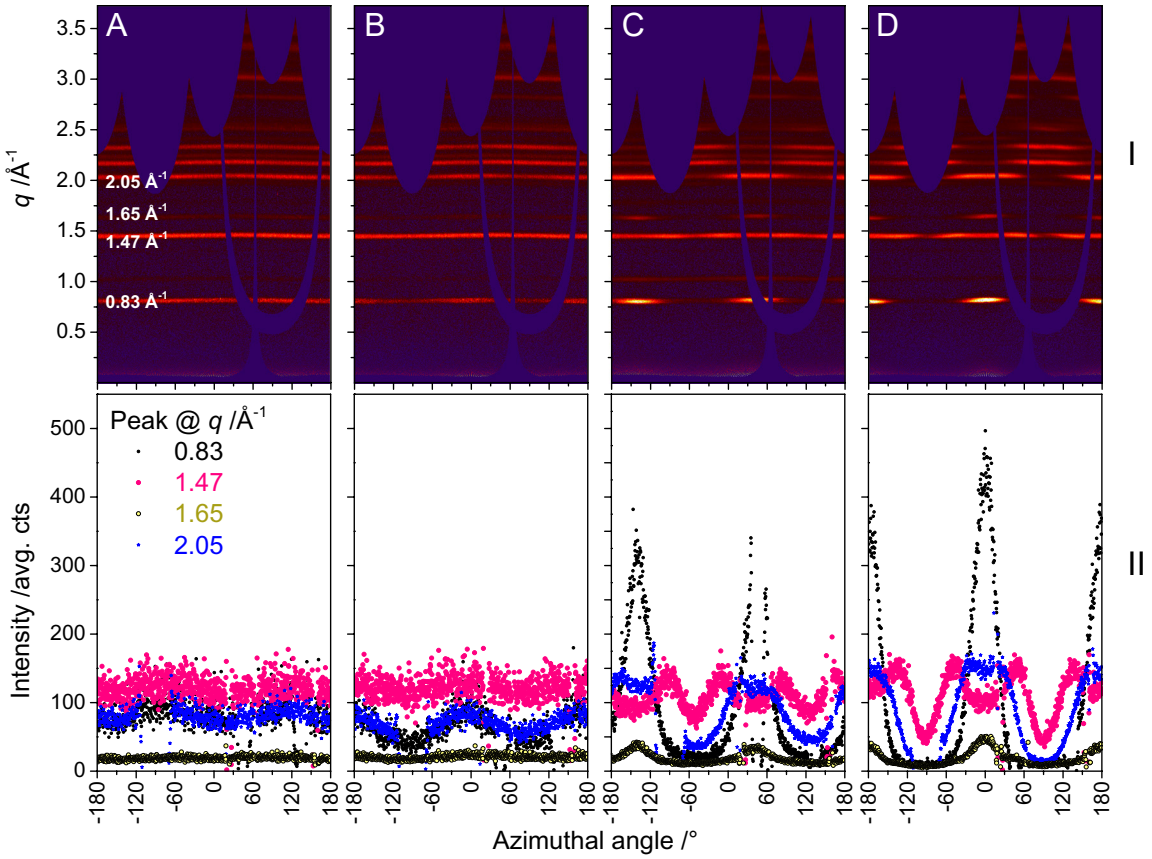

Fig. 3. Diffraction patterns derived from the *Koshteh* plaster during its preparation at different stages of mechanical processing (*Methods* and Movie S1); (*A*) 0 min, (*B*) 2 min, (*C*) 4 min, and (*D*) 8 min. Row I: diffraction patterns are given in polar coordinates (cake plots), and the *q* positions of characteristic peaks are labeled. Row II: integrated profiles for each of the characteristic peaks at position *q*.

a nonparametric test, which did not require a normal distribution. We used the Kruskal–Wallis test (48) (*SI Appendix*: Supplementary Note 2, Table S1), which enabled us to compare two or more independent samples. The results of this statistical test for the CH_3-tip (hydrophobic tip) revealed a significant difference in at least one of the samples with 95% significance (*P*-value < 2.2e−16). This is the case of the *Sottile* sample, which has a large tail in the region of high adhesion values indicating its more hydrophobic

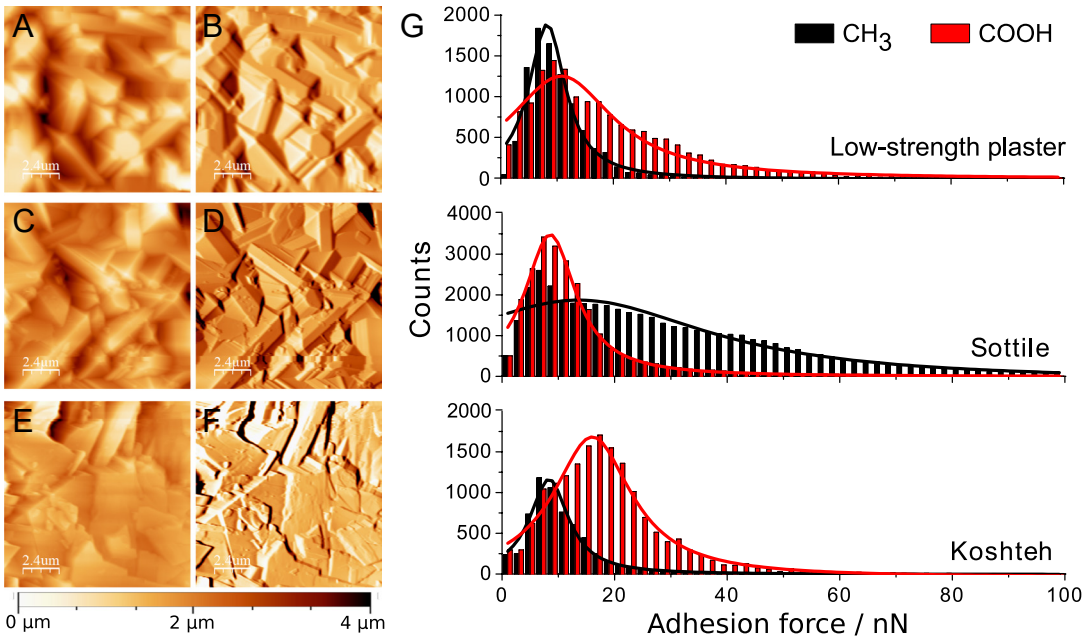

Fig. 4. Height (*Left*) and deflection (*Right*) images acquired in low-strength regular plaster (*A* and *B*), *Sottile* (*C* and *D*), and *Koshteh* (*E* and *F*) samples using CH_3- and COOH-tips. (*G*) Adhesion force histograms of each sample obtained with CH_3- (black histograms) and COOH-tips (red histograms). Each histogram corresponds to the adhesion force data obtained from 20 force maps (18,000 force–distance curves).

behavior (Fig. 4*G*). Furthermore, a Wilcoxon signed-rank test (49) (*SI Appendix*, Supplementary Note 2, Table S1) was used to compare the hydrophobicity between *Koshteh* and regular plaster, which resulted in a *P*-value of 0.17 (*SI Appendix*, Table S1), with 95% significance. The mean equality was accepted, and thus, there were no significant differences between both samples. Finally, the Kruskal–Wallis test was performed on the data obtained with the COOH-tip (hydrophilic tip). We also confirmed that the *Sottile* sample was significantly different from the other two samples when using the hydrophilic tip (*P*-value < 2.2e−16, *SI Appendix*, Table S1). However, the Wilcoxon signed-rank test rejected the mean equality between *Koshteh* and low-strength plaster regarding the hydrophilic behavior (*P*-value = 2.969e−11, *SI Appendix*, Table S1). Therefore, we can conclude that significant differences exist between the samples, where the *Koshteh* sample is the most hydrophilic, which is attributed to the predominance of the hydrophilic {010} facet. On the other hand, the *Sottile* sample was the most hydrophobic and low-strength plaster falling in the middle—with both predominantly being formed of needle-shaped crystals, with relatively smaller {010} facets.

Discussion

The results presented above reveal that the preparation protocol of gypsum plasters can lead to unique microstructural characteristics. Low-strength plaster is characterized by randomly oriented, predominantly needle-shaped, gypsum crystals (Fig. 1*A*). In the case of the *Gesso Sottile*, the high-dilution and long reaction times, required for the Italian paste preparation method, promote a low number density of crystal nuclei growing at low supersaturations close to equilibrium. Under such conditions, crystals grow larger with long equilibration periods promoting the dissolution of smaller crystallites to feed the growth of larger ones (i.e., Ostwald ripening). The optional water exchange step, as is also reported in the literature (13, 14, 16), would temporarily push the system into undersaturation, which should further promote the dissolution of smaller crystallites, and thus allow for the further growth of larger ones. High dilution conditions, on the other hand, can have a negative impact on the final strength of the solidified material. As such, the resulting material is rather loosely packed compared with a regular gypsum paste, in which the final strength is associated with the interlocking of gypsum needles (2).

The most stark difference between the preparation of *Gach-e Koshteh* and a typical plaster of Paris is the mechanical treatment that takes place with this traditional recipe (Movie S1). However, it should also be noted that the water/plaster ratio (W/P) of *Koshteh* is at least twice that of a typical gypsum plaster. The extensive mechanical treatment during the hydration of *Koshteh* paste removes the interlacing network and breaks down the larger needle-shaped crystals predominantly along their elongated direction. Since these long needles also continuously grow in other directions, following specific crystallographic directions of the fracturing process guide them toward a more platelet shape of gypsum crystals (Fig. 1*C*). Hence, the interlacing network of gypsum needles, characteristic for a regular hardened gypsum plaster, is replaced by preferentially oriented platelets. This microstructure transformation is observable in the 2D diffraction patterns of our time-resolved series, which exhibit the gradual transition from low-strength gypsum paste at the beginning to a *Koshteh* material at the end (Fig. 3). The mechanical processing also leads to compacting of the material evidenced by a ~22% decrease in porosity with respect to the first sample of (0-min interval) similar to low-strength plaster with a W/P equal to 1 (26) (*SI Appendix*, Fig. S3), which is further enhanced by the better-fitting platelet shape of the crystals. All this takes place continuously during the squeezing and smashing processes, breaking large and constantly growing crystals and disrupting the interlocking network, while forcing gypsum crystals to be laid on top of each other parallel to their {010} faces.

Importantly, the engineering of the microstructure associated with *Sottile* and *Koshteh* results in a characteristic nanoscale topography and directly impacts the wetting properties of the final material. AFM imaging showed that platelet-shaped crystals are preferentially oriented with their {010} faces parallel to the external plaster surface. AFS measurement on this surface revealed that *Koshteh* paste is more hydrophilic compared with regular paste and *Sottile*, both showing a much higher degree of randomly oriented needle-shaped crystals. This link between crystal shape/ordering and surface wetting properties is a direct consequence of the wetting behavior of the different crystallographic faces of gypsum. The {010} face displays the most hydrophilic character of all gypsum faces due to the double layer of structural water of the {010} face (50). In the case of *Koshteh*, this hydrophilic character is translated to the plaster surface via a double route: first, the morphology of the crystals is tuned so that the area of the {010} face is maximized with respect to needle-shaped crystals forming regular plaster (Fig. 1), and second, the crystals are preferentially ordered in such a way that the {010} face is parallel to the external plaster surface (Figs. 2 and 3).

We showed that for gypsum-based materials *Koshteh* and *Sottile,* intentional processing was required to engineer the crystal structure so that desired microstructural properties (size of crystals and their local orientations) would be manifested. People in the past did not have analytical tools that we employed to identify the microstructural differences among the gypsum pastes, nor did they necessarily even consider the concept of a microstructure. Nevertheless, they were able to (partially) correlate the preparation method with the macroscopic properties of the final material. *Koshteh* was probably developed in the 13th-14th centuries AD to counter several problems faced by stucco masters in Persia when preparing a smooth substrate for mural paintings or developing some advanced stucco decoration techniques (28). Typical gypsum paste is quick setting if the W/P ratio is low (W/P = 30 to 50 wt%). However, in such a case, the obtained plaster cannot be used as a finishing layer since it hardens too quickly without yielding the smooth finishing surface necessary for posterior pigmentation. The workability time of the plaster is increased if the W/P ratio is high (W/P = 100 to 300 wt%), which allows for a smooth surface to be prepared, although the resulting plaster is very weak and highly prone to mechanical damage. To resolve these issues, additional surface preparation for pigmentation was required to improve its smoothness and strength. One solution to this problem was to mix *Sottile,* or other white pigments, with a binder phase, usually animal glue, and use this composite material as a substrate/primer for painting (16). In this regard, the approach in *Koshteh* is radically different, relying on the tailored microstructure of the plaster to provide the required smoothness and adhesion of layers, avoiding the use of any type of glue. While the aspect of improved adhesion of layers is not investigated in this work, it is often mentioned by traditional craftspeople (*SI Appendix*, Text 1).

The preparation of *Koshteh* is a labor-intensive process, in which a trained craftsperson is required to press and squeeze all parts of the paste simultaneously to ensure that crystallization comes to completion in all the parts of the treated volume simultaneously. Otherwise, one might produce a small volume of untreated stiff paste, which would be detrimental to the final artwork. Processing becomes increasingly demanding toward the end of the plaster setting, and typically, in a single batch, approximately 2 to 3 kg of the *Koshteh*

paste can be produced by a stucco master (note: we made ~100 g in a single experiment). The processing of our paste (Movie S1) is quite exothermic as occurs with the setting process of plaster of Paris (6). The released heat has been used as an intrinsic indicator for stucco masters, which marks the onset of consecutive stages and their duration during the processing of *Koshteh*. Crucially, when the exothermic stage is over, the paste will start to cool down, and a thin layer of water will appear on the surface of the paste (*SI Appendix*, Text 1). This indicates the time at which the *Koshteh* paste is ready for use and is characterized by its slightly whiter appearance, soft texture, and a long-term workability with enhanced wettability. The as-described mechanical treatment is also the origin of the *Gach-e Koshteh* name: so-to-speak "the alive and strong body" of gypsum plaster was "killed."

Taking advantage of the characteristic microstructure of *Gach-e Koshteh*, we also investigated several historical stucco samples collected from different monuments in Iran, two of them (StB-102, *SI Appendix*, Figs. S5, S7, and S8 *C* and *D*; and StB-27, *SI Appendix*, Figs. S6, S7, and S8 *A* and *B*), preserving certain microstructural *Koshteh* features after more than six centuries. The walls of the dome chamber of the *Sheikh Ahmad-e Jami* mausoleum complex are covered by geometrical and floral wall painting from the 14th century AD, executed on a thin layer, 2 to 3 mm thick, of gypsum plaster covering more than 150 m^2 of wall and presumed to be made of a *Koshteh* paste (27). Over the centuries, these wall paintings were exposed to environmental deterioration which was countered by several stages of conservation and restoration processes. Due to the consolidation of these wall paintings, the thin *Koshteh* underlayer, containing modern polymers, exhibits X-ray diffraction patterns with the features of regular gypsum plaster (*SI Appendix*, Fig. S5*A*). Nonetheless, the typical microstructure of plate-like crystals, representative of the *Koshteh* layer, could still be partially observable in SEM (*SI Appendix*, Fig. S5 *A–D*). This discrepancy is caused by the fact that SEM probes only a small volume of the sample, up to several hundred μm^3, while XRD delivers average information from several mm^3. The edges of the crystals in most parts of the microstructure are damaged and/or rounded, which is expected since these parts are the most reactive sites of a crystal and more prone to, e.g., dissolution in water. There are, however, some parts of the historical plaster that survived without apparent sign of weathering (*SI Appendix*, Fig. S5*D*). Overall, the plaster shows a compact structure with a preferred orientation along the {010} faces of gypsum comparable with the microstructure of the *Koshteh* paste prepared in the laboratory. Additional evidence of the *Koshteh* recipe has survived through traditional masters from the Isfahan and Yazd region in central Iran (*SI Appendix*, Text 1). One of these stucco masters (Khalil Kargar) described the production process of *Appliqué* plaster decoration (*Fetilehey*) in the *Sayyid Rukn al-Din* mausoleum from the Ilkhanid period (28). According to this master, the stucco technique in Yazd required a half-*Koshteh* paste, which is most likely structurally comparable with ~2 to 4 min of our time-resolved series (Fig. 3). The XRD from this paste again shows characteristics of regular gypsum plaster (*SI Appendix*, Fig. S6*A*), but the SEM micrographs (*SI Appendix*, Fig. S6 *B* and *C*) indicate that this sample has local orientation mixed with interlocked needle-shaped crystals of gypsum in the microstructure. This combination, which is also mixed with polysaccharide glue (plant-based glue similar to gum arabic), provides an example of soft paste with long workability (28), which does not lose its strength, even if deposited as a layer of up to ~20 mm in thickness. In addition, Khalil Kargar (*SI Appendix*, Text 1) also mentioned that in a half-*Koshteh* recipe, used for this decoration, the plaster of Paris was mixed with clay before being mixed with water. Indeed, *SI Appendix*, Fig. S7 shows that half-*Koshteh* StB-27 (from *SI Appendix*, Fig. S6) contains a clay admixture, in agreement with the testimony, where the clay has a basal spacing of 1.2 nm. However, it is important to highlight that in its essence the half-*Koshteh* method does not necessarily involve mixing with clay or polysaccharide but rather refers to the actual partially mechanical treatment.

The two presented historical examples of plausible applications of a *Koshteh* technique also highlight the difficulties related to the unequivocal characterization and classification of gypsum-based archeological materials. The laboratory-prepared replicas seem to constitute the best-case scenarios for the microstructural features present in gypsum and as such allowed us to establish a link between the preparation method, the morphology of the gypsum crystals, and expected properties such as wettability or porosity. However, gypsum is a rather soluble (2.0 to 2.5 g/l at 25 °C) and soft material (2 on the scale of Mohs for single crystals of gypsum) and is thus prone to alterations, especially at the microstructural level due to abrasion or partial dissolution. Those changes can be very rapid, but at the same time, they may leave hardly any macroscopically observable indications that the material has been altered. Consequently, historical samples will typically contain only partial microstructural features pointing to a particular preparation technique. Moreover, the particular plaster microstructure, be it *Sottile* or *Koshteh*, serves its purpose, in the short-term, only at the moment of preparation of a decoration when the gypsum material is deposited and soon after. The long-term preservation of the specific microstructure of the gypsum plaster is unclear, but this was also not required in practical terms. In other words, the external appearance of various gypsum plasters is quite similar, but the early preparation stages do matter for interactions with, e.g., paints.

Outlook

The physicochemical characterization of the properties of specific gypsum plasters/substrates prepared through distinct methods is paramount to establishing effective conservation and restoration strategies of heritage objects containing calcium sulfate. Our research sheds light on the microstructure of three gypsum-based recipes and demonstrates their differences in wettability, density, and crystallographic characteristics, which would dictate their behavior upon deterioration by water. On the other hand, in modern conservation techniques for cultural heritage, a wide variety of polymers, such as polyvinyl acetate, acrylic resins, e.g., Paraloid B72, or water-dispersed acrylic resins, e.g., Primal AC-33 (51), with different solvent and physicochemical characteristics, are applied to consolidate an object or a decoration. The combination of our as-presented perspective on how the microstructure and wetting properties of the same material (gypsum) can change through application of a particular recipe in combination with a knowledge and practice on how various polymers/solvents might interact with gypsum-based objects can guide strategies to select the best conservation and restoration practices. Such strategies could deploy various polymers/solvents in accordance to how they may interact with specific gypsum-based objects, potentially leading to more sustainable preservations. For example, the choice of a consolidation polymer that should be used in combination with *Sottile* or *Koshteh* would depend on matching hydrophobic/hydrophilic interactions so that sufficient penetration and binding of the polymer with the gypsum crystals could be achieved. On a practical level, there is still a need for well-designed experiments. In this regard, our laboratory-based replicas constitute a relevant testing ground for the unrestricted assessment of such polymeric binders before an actual application of different polymers to valuable historical cultural materials. The unraveling of these historical techniques is also potentially relevant for the development of the next generation of gypsum-based construction applications, such as plasterboards. In these materials, their strength, porosity, wettability, and overall durability could be tuned by alternating

the microstructure of consequent gypsum layers (i.e., to yield a pseudocomposite material). For example, by simple microstructural engineering, one could obtain plasterboards, which are more resistant to water damage, while at the same time, they could contain layers allowing for easy painting without the use of primers. Nevertheless, these hypothetical concepts indeed need further research and other microstructural aspects such as the influence of porosity require in-depth consideration.

Conclusion

The laboratory-reproduced gypsum plaster preparation methods constitute examples of microstructural engineering developed and implemented in the premodern era. They are highly unique in this respect because crystal engineering was applied to nonmetallic materials. In the course of material processing, we showed that the morphology of the crystals can be adjusted so that either needles or plates are obtained. As a result of this morphology tuning, a shift in average nanoscale hydrophobic and hydrophilic interactions of plaster "surfaces" is induced. The increase in hydrophilicity seen for plates with respect to needles was caused by the maximization of the {010} facets of gypsum, which is known to be more wettable. These subtle adjustments to plaster microstructures are arguably difficult to observe macroscopically in aged materials and are less long lasting due to the fragility of gypsum. Notwithstanding, they play a crucial primary role during application of the plaster and its posterior treatment (e.g., decoration).

Data, Materials, and Software Availability. All study data are included in the article and/or *SI Appendix*.

ACKNOWLEDGMENTS. The German Research Foundation (DFG) supported this research as a part of the project "Aesthetics of Stucco and Tiles" in the Islamic Art and Archaeology at the University of Bamberg (DFG project number 399216810). We are thankful to Prof. Lorenz Korn, University of Bamberg, for his valuable help and support during this DFG project. We kindly acknowledge Sigrid Benemann (BAM), Vasile-Dan Hodoroaba (BAM), and Sathish Mayanna (ZEISS Microscopy) for performing SEM analysis of selected samples. We also acknowledge Carsten Prinz (BAM) and Annett Zimathies (BAM) for the gas sorption and porosimetry measurements.

Author affiliations: [a]Otto-Friedrich-Universität Bamberg, Islamic Art and Archaeology, Bamberg 96047, Germany; [b]Université Grenoble Alpes, Université Savoie Mont Blanc, CNRS, Institut de Recherche pour le Développement (IRD), Institut Français des Sciences et Technologies des Transports, de l'Aménagement et des Réseaux (IFSTTAR), Institute de Sciences de la Terre (ISTerre), Grenoble F-38000, France; [c]Instituto Andaluz de Ciencias de la Tierra, Consejo Superior de Investigaciones Científicas (CSIC)—University of Granada, Granada 18100, Spain; and [d]Federal Institute for Materials Research and Testing (BAM), Berlin 12489, Germany

1. A. E. S. Van Driessche, T. M. Stawski, M. Kellermeier, Calcium sulfate precipitation pathways in natural and engineered environments. *Chem. Geol.* **530**, 119274 (2019).
2. N. B. Singh, B. Middendorf, Calcium sulphate hemihydrate hydration leading to gypsum crystallization. *Prog. Crys. Growth Charact. Mater.* **53**, 57–77 (2007).
3. A. Saha *et al.*, New Insights into the transformation of calcium sulfate hemihydrate to gypsum using time-resolved cryogenic transmission electron microscopy. *Langmuir* **28**, 11182–11187 (2012).
4. Y. Tang, J. Gao, C. Liu, X. Chen, Y. Zhao, Dehydration pathways of gypsum and the rehydration mechanism of soluble anhydrite γ-CaSO4. *ACS Omega* **4**, 7636–7642 (2019).
5. J. Adrien, S. Meille, S. Tadier, E. Maire, L. Sasaki, In-situ X-ray tomographic monitoring of gypsum plaster setting. *Cement Concrete Res.* **82**, 107–116 (2016).
6. H. B. Weiser, F. B. Moreland, The setting of plaster of paris. *J. Phys. Chem.* **36**, 1–30 (1932).
7. W. David Kingery, P. B. Vandiver, M. Prickett, The beginnings of pyrotechnology, part II: Production and use of lime and gypsum plaster in the pre-pottery neolithic Near East. *J. Field Archaeol.* **15**, 219–243 (1988).
8. A. Lucas, J. Harris, *Ancient Egyptian Materials and Industries* (Courier Corporation, 2012).
9. M. Philokyprou, "The earliest use of lime and gypsum mortars in cyprus" in *Historic Mortars*. J. Válek, J. J. Hughes, C. J. W. P. Groot, Eds. (*RILEM Bookseries*, Springer, Netherlands, 2012), pp. 25–35.
10. M. Svoboda, C. Cartwright, Eds., *Mummy Portraits of Roman Egypt: Emerging Research from the APPEAR Project* (J. Paul Getty Museum, Los Angeles Getty Publications, ed. 1, 2020).
11. D. K. Strahan, Special studies: Naturally deposited versus intentionally applied gypsum on archaeological materials from Harappa. Pakistan. *J. Field Archaeol.* **18**, 527–530 (1991).
12. G. Gariani *et al.*, First insights on the mineral composition of "stucco" devotional reliefs from Italian Renaissance Masters: Investigating technological practices and raw material sourcing. *J. Cult. Heritage* **34**, 23–32 (2018).
13. C. Cennini, *Il libro dell'arte*, F. Brunello, Ed. (Neri Pozza, Vicenza, 1971).
14. R. J. Gettens, M. E. Mrose, Calcium sulphate minerals in the grounds of italian paintings. *Studies Conserv.* **1**, 174–189 (1954).
15. P. Cardoso Isabel, E. Pye, Preparing the foundation for stable gilding: Baroque craftsmen's empirical understanding of gesso gilding grounds. *J. Archaeol. Sci.* **79**, 96–106 (2017).
16. S. S. Gomez *et al.*, "Reconstruction of documented preparation methods for gesso grosso and gesso sottile in Spanish School panel paintings" in *Art Technological Research: Towards a New Discipline* (Archetype Publications, 2008), pp. 178–181.
17. A. Conti, H. Glanville, *History of the Restoration and Conservation of Works of Art* (Routledge, 2007).
18. J. Kröger, G. Kröger-Hachmeister, *Sasanidischer Stuckdekor: Ein Beitrag zum Reliefdekor aus Stuck in sasanidischer und frühislamischer Zeit nach den Ausgrabungen von 1928/9 und 1931/2 in der sasanidischen Metropole Ktesiphon (Iraq) und unter besonderer Berücksichtigung der Stuckfunde vom Taḫt-i Sulaimān (Iran), aus Niẕāmābād (Iran) sowie zahlreicher anderer Fundorte* (von Zabern, 1982).
19. A. U. Pope, P. Ackerman, *A Survey of Persian Art, from Prehistoric Times to the Present: Introductory Essays, Pre-Achaemenid, Achaemenid and Parthian Periods* (Published under the auspices of the Asia Institute of Pahlavi University, 1967).
20. A. Shekofteh, O. Oudbashi, Chemical and microscopic investigation of ancient mortar and plaster from the middle elamite period Tepti Ahar's Vaulted tomb, Southwestern Iran. *Int. J. Arch. Heritage* **14**, 1269–1283 (2020).
21. M. Mishmastnehi, The application of crystallographic interpretation on technical study of gypsum-based historical materials (case studies of stucco decoration of Kuh-e Khwaja and Gypsum Mortars from Shadiakh and Alamut). *J. Res. on Archaeometry* **1**, 1–14 (2016).
22. H. Aslani, Arayae-ha-yi gachi dar memari-i dawrah-i Islami-i Isfahan (Pazhuheshgah-i Farhang Honar va Ertebatat, 2014).
23. R. B. Heimann, M. Maggetti, *Ancient and Historical Ceramics* (Schweizerbart Science Publishers, 2014).
24. B. W. Roberts, C. P. Thornton, *Archaeometallurgy in Global Perspective: Methods and Syntheses* (Springer, 2014).
25. J. Henderson, *Ancient Glass: An Interdisciplinary Exploration* (Cambridge University Press, 2013).
26. M. Mucha, P. Mróz, D. Wrona, P. Konca, J. Marszałek, Microstructural formation of gypsum by setting in the presence of hydroxypropyl methylcellulose (HPMC). *J. Therm. Anal. Calorim.* **147**, 1107–1113 (2022).
27. H. Sayyadshahri, "Technical study and documentation of the paintings from the dome-chamber of Sheikh Ahmad-e Jami mausoleum,"Unpublished master's thesis in the field of Conservation and Restoration of Cultural properties, University of Art, Tehran (2009).
28. E. Alvandian Khakbaz, "Production process identification of unique stucco decoration from Ilkhanid monument, Roknieh, in Yazd, [Iran]" *Proceedings of the 8th Conference on the Conservation and Restoration of Historical-Cultural Objects and Architectural Decorations* (Tehran: Sazman-e Miras-e Farhangi, Sanai-e Dasti va Gardeshgari, 2012), pp. 159–175.
29. G. J. Smales, B. R. Pauw, The MOUSE project: A meticulous approach for obtaining traceable, wide-range X-ray scattering information. *J. Inst.* **16**, P06034 (2021).
30. M. Basham *et al.*, Data analysis WorkbeNch (DAWN). *J. Synchrotron Rad.* **22**, 853–858 (2015).
31. J. Filik *et al.*, Processing two-dimensional X-ray diffraction and small-angle scattering data in DAWN 2. *J. Appl. Cryst.* **50**, 959–966 (2017).
32. T. M. Stawski *et al.*, Seeds of imperfection rule the mesocrystalline disorder in natural anhydrite single crystals. *Proc. Natl. Acad. Sci. U.S.A.* **118**, e2111213118 (2021).
33. A. B. Rodriguez-Navarro, Registering pole figures using an X-ray single-crystal diffractometer equipped with an area detector. *J. Appl. Cryst.* **40**, 631–634 (2007).
34. A. B. Rodriguez-Navarro, XRD2DScan: New software for polycrystalline materials characterization using two-dimensional X-ray diffraction. *J. Appl. Cryst.* **39**, 905–909 (2006).
35. J. L. Hutter, J. Bechhoefer, Calibration of atomic-force microscope tips. *Rev. Sci. Instrum.* **64**, 1868–1873 (1993).
36. J. C. Love, L. A. Estroff, J. K. Kriebel, R. G. Nuzzo, G. M. Whitesides, Self-assembled monolayers of thiolates on metals as a form of nanotechnology. *Chem. Rev.* **105**, 1103–1170 (2005).
37. I. Horcas *et al.*, WSXM: A software for scanning probe microscopy and a tool for nanotechnology. *Rev. Sci. Instrum.* **78**, 013705 (2007).
38. C. T. Rueden *et al.*, Image J2: ImageJ for the next generation of scientific image data. *BMC Bioinformatics* **18**, 529 (2017).
39. S. Brunauer, P. H. Emmett, E. Teller, Adsorption of gases in multimolecular layers. *J. Am. Chem. Soc.* **60**, 309–319 (1938).
40. E. W. Washburn, The dynamics of capillary flow. *Phys. Rev.* **17**, 273 (1921).
41. P. E. Grattan-Bellew, Effects of preferred orientation on X-ray diffraction patterns of gypsum. *American Mineral. J. Earth Planet. Mater.* **60**, 1127–1129 (1975).
42. R. C. Hildyard, D. J. Prior, E. Mariani, D. R. Faulkner, Crystallographic preferred orientation (CPO) of gypsum measured by electron backscatter diffraction (EBSD). *J. Microscopy* **236**, 159–164 (2009).
43. J. E. Manson, Preferred orientation of platelets in X-ray diffractometer powder samples. *J. Appl. Phys.* **26**, 1254–1256 (1955).
44. O. Dos Santos Ferreira, E. Gelinck, D. de Graaf, H. Fischer, Adhesion experiments using an AFM–Parameters of influence. *Appl. Surface Sci.* **257**, 48–55 (2010).
45. F. Marinello, S. Carmignato, A. Voltan, E. Savio, L. De Chiffre, Error sources in atomic force microscopy for dimensional measurements: Taxonomy and modeling. *J. Manufacturing Sci. Eng.* **132** (2010).
46. X. Tian *et al.*, AFM characterization of surface mechanical and electrical properties of some common rocks. *Int. J. Min. Sci. Technol.* **32**, 435–445 (2022).
47. B. Sauerer *et al.*, Quantifying mineral surface energy by scanning force microscopy. *J. Colloid Interface Sci.* **472**, 237–246 (2016).
48. W. H. Kruskal, W. A. Wallis, Use of ranks in one-criterion variance analysis. *J. Am. Stat. Assoc.* **47**, 583–621 (1952).
49. F. Wilcoxon, Individual comparisons by ranking methods. *Biomet. Bull.* **1**, 80–83 (1945).
50. J. C. Santos, F. R. Negreiros, L. S. Pedroza, G. M. Dalpian, P. B. Miranda, Interaction of water with the gypsum (010) surface: Structure and dynamics from nonlinear vibrational spectroscopy and ab initio molecular dynamics. *J. Am. Chem. Soc.* **140**, 17141–17152 (2018).
51. V. Horie, *Materials for Conservation: Organic Consolidants, Adhesives and Coatings* (Butterworth-Heinemann, Burlington, MA, ed. 2, 2010).